Protocol for hybrid entanglement between a trapped atom and a quantum dot

Edo Waks and C. Monroe
Joint Quantum Institute, University of Maryland and National Institute of Standards and Technology, College Park, Maryland 20742, USA

(Received 6 July 2009; published 30 December 2009)

We propose a quantum optical interface between an atomic and solid-state system. We show that quantum states in a single trapped atom can be entangled with the states of a semiconductor quantum dot through their common interaction with a classical laser field. The interference and detection of the resulting scattered photons can then herald the entanglement of the disparate atomic and solid-state quantum bits. We develop a protocol that can succeed despite a significant mismatch in the radiative characteristics of the two matter-based qubits. We study in detail a particular case of this interface applied to a single trapped $^{171}Yb^{+}$ ion and a cavity-coupled InAs semiconductor quantum dot. Entanglement fidelity and success rates are found to be robust to a broad range of experimental nonideal effects such as dispersion mismatch, atom recoil, and multiphoton scattering. We conclude that it should be possible to produce highly entangled states of these complementary qubit systems under realistic experimental conditions.

DOI: 10.1103/PhysRevA.80.062330 PACS number(s): 03.67.Bg, 03.65.Ud

I. INTRODUCTION

Quantum entanglement, long considered to be the most puzzling aspect of quantum mechanics [1,2], is now realized to be a potential resource for enhanced processing and communication of information. The field of quantum-information science exploits quantum entanglement for tasks that are otherwise impossible or inefficient using conventional information processing approaches [3]. Recent advances in the control of physical systems, ranging from isolated atoms and photons to individual degrees of freedom in condensed matter, have shown great promise in the development of quantum-information hardware [4].

The majority of work to date has been centered around entanglement of identical quantum systems such as identical atoms and photons. There is great interest in extending entanglement over disparate quantum systems. Such hybrid entanglement can exploit advantages of each individual system to enhance capabilities of quantum technology. An important example is the hybrid entanglement between matter and photonic quantum systems. This type of entanglement, which has been demonstrated using both trapped ions [5] and atomic ensembles [6], enables one to combine the advantages of the long coherence times of atomic systems with the ability of photonic systems to transport quantum information. Another important example is the recent entanglement of two different species of trapped atomic ions, where one species (Al^{+}) has excellent coherence properties and the other (Be^{+}) allows efficient qubit measurement [7].

Here, we theoretically investigate the possibility of creating hybrid entanglement between semiconductor and atomic quantum systems. Specifically, we propose a protocol for entangling a quantum dot (QD) in a microcavity with a trapped atom through a common photonic interaction. Such hybrid entanglement is expected to stimulate new concepts for distributed quantum computation that exploit the long coherence times of trapped ions with the fast dynamics and strong atom-photon interactions of a QD. We show that a common photonic channel can link these disparate systems to achieve hybrid-matter quantum entanglement despite significant mismatches between atomic and semiconductor qubits.

Photon mediated entanglement has been proposed for entangling like systems such as atoms [6,8], nitrogen-vacancy (N-*V*) centers in diamond [9], and cavity-coupled QDs [10,11]. It has been experimentally demonstrated between trapped ions [12] and atomic ensembles [13–15]. To extend such ideas to entangle different matter qubits requires a protocol that is robust to significant mismatch in spectral and temporal properties. In this paper we propose such a protocol in which the atomic system is coupled to a free-space field by elastic scattering, while the QD is coupled via cavity interaction. We extensively investigate a particularly promising implementation of this protocol in which an electrostatically trapped $^{171}Yb^{+}$ ion is entangled with a cavity-coupled indium arsenide (InAs) QD. We address the central challenges in realizing this hybrid quantum link, including the mismatch in the optical spectra of these systems and decoherence processes that are particular to each node of the hybrid circuit. In particular, we analyze in detail "which-path" decoherence due to atom recoil and multiphoton scattering and derive an analytical expression for entanglement fidelity and entanglement rate.

In Sec. II, we give a low-level description of the proposed entanglement protocol. Section III provides detailed calculations of the atom scattering amplitudes, and analyzes the effect of dispersion. Section IV considers atom motion and recoil, and calculates the fidelity under realistic experimental conditions. In Sec. V we consider the effects of leakage of which-path information due to multiphoton scattering. The final section investigates the validity of the weak excitation approximation which is extensively used to calculate both atomic scattering and reflection from the cavity-QD system.

II. BASIC PROTOCOL

Figure 1(a) illustrates the proposed method for entangling a QD with an atom. The QD is coupled to a resonant microcavity while the atom is electromagnetically confined at a

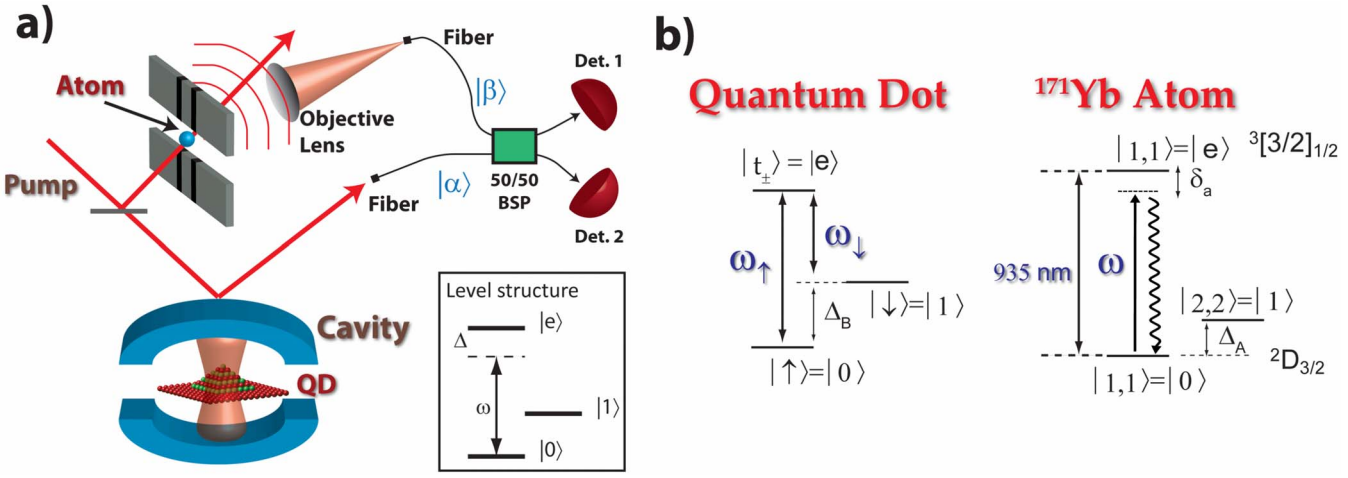

FIG. 1. (Color online) (a) Proposed setup for entangling an atom with a QD. A trapped atom and a cavity-coupled QD are held at different spatial locations. Both QD and atom have a level structure shown in the inset, and a common pump beam excites both systems. The reflected light from the cavity is mixed with the scattered light from the atom on a 50-50 beamsplitter. Path lengths are set for constructive interference at detector 1. A detection event at detector 2 places the two systems in an entangled state. (b) Specific level structure for the QD and atom. The spin states of a singly charged QD can serve to create the desired qubit states, while the positive or negative trion state ($|t_{\pm}\rangle$) serves to couple the qubit to the cavity. The two qubit states are split in energy by Δ_B due to an applied magnetic field. For the atom we consider the specific example of a $^{171}Yb^{+}$ ion and use the hyperfine $|1,1\rangle$ and $|2,2\rangle$ states (with hyperfine splitting Δ_A=0.86 GHz) in the $^2D_{3/2}$ manifold to store quantum information. The atom scatters a linearly polarized input when in the $|1,1\rangle$ state, while the $|2,2\rangle$ state does not scatter this light due to selection rules.

remote location. Each system consists of a qubit represented by the two states, $|0\rangle$ and $|1\rangle$, where state $|0\rangle$ is coupled to a third excited state $|e\rangle$ via an optical transition. We consider the case where this transition in the QD and atom occur at similar (not necessarily identical) optical wavelengths. The entanglement method we consider is general, and can apply to a broad range of atomic and semiconductor systems. However, to perform calculations we specialize to the case of an InAs QD that is entangled with an electrostatically trapped $^{171}Yb^{+}$ ion. The assumed level structure for these two qubit systems is shown in Fig. 1(b). We focus on $^{171}Yb^{+}$ because of its optical $^2D_{3/2}$ to $^3[3/2]_{1/2}$ transition, which occurs at 935 nm and is therefore compatible with the near infrared transition wavelength of InAs QDs. For the QD, the qubit states can reside in the Zeeman split spin states of a single charge carrier, with an optical coupling to an excited trion state, as recently demonstrated [16,17]. The loading of a single spin into a microcavity coupled QD has also been recently achieved [18]. For the atom, the qubit states are represented by long-lived electronic or nuclear hyperfine states, with an optical coupling to a dipole-allowed excited electronic state [19]. We consider the hyperfine qubit states residing in the metastable $^2D_{3/2}$ level, with a coupling to the excited $^3[3/2]_{1/2}$ level at 935 nm [20].

Entanglement is established by first initializing the state of each of the two qubits to superposition state $|\psi_i\rangle=(|0\rangle+|1\rangle)/\sqrt{2}$. The QD system can be initialized using experimentally demonstrated single [21] and two-laser coherent control techniques [16,17], while the atom can be controlled using optical pumping and microwave or stimulated Raman transitions [19,20]. Following initialization, a laser pulse is coherently split into two components directed to the two quantum systems. One of the components is reflected off of the cavity containing a QD while the second component drives the atom off resonance, resulting in an elastically scattered field that is phase coherent with the input field. Phase coherence of the elastically scattered component has been experimentally verified through Young's interference [22], and has also been theoretically investigated [23]. We define $|\alpha\rangle$ as the coherent field reflected from the cavity, and $|\beta\rangle$ as the field elastically scattered from the atom. The two fields are combined on a beamsplitter whose path lengths are set for constructive interference at detector 1 [shown in Fig. 1(a)], requiring optical interferometric stability over the system. A detection event at detector 2 will collapse the state of the atom and QD into an entangled state.

To understand the entanglement formation process, we first assume that both the scattered field from the ion and the reflected field from the cavity are quasimonochromatic, phase coherent, and sufficiently weak that they can be expanded to first order in photon number. In later sections we will derive the entanglement fidelity under more realistic experimental conditions. We define $\omega_{\uparrow}$ and $\omega_{\downarrow}$ as the trion resonant frequencies for the two different spin states of the charged QD, which are detuned by Δ_B due to an applied external magnetic field. The cavity resonant frequency is defined as ω_c, and input field frequency as ω. The reflection coefficient r and transmission coefficient t of the cavity are [10,24,25]

$$r(\omega) = \frac{-i\Delta + \mathcal{CL}(\delta_{qd}, \gamma_{qd})}{1 - i\Delta + \mathcal{CL}(\delta_{qd}, \gamma_{qd})}, \tag{1}$$

$$t(\omega) = \frac{1}{1 - i\Delta + \mathcal{C}\mathcal{L}(\delta_{qd}, \gamma_{qd})}, \tag{2}$$

where $\delta_{qd}=\omega_c-\omega_\uparrow$ is the detuning between the cavity and the QD and $\Delta=(\omega-\omega_c)/\kappa$ is the laser-cavity detuning scaled to the cavity linewidth κ. The QD exciton decay rate is given by γ_{qd}, $\mathcal{C}=4g^2/(\gamma_{qd}\kappa)$ is the QD-cavity cooperativity, g is the QD-cavity coupling strength, and $\mathcal{L}(\delta,\gamma)=\gamma/(\gamma-i\delta)$ is a Lorentzian profile [10].

The incident field is set to be resonant with the cavity $(\omega=\omega_c)$ so that $\Delta=0$. We also set $\omega_\uparrow=\omega_c$ so that the QD is resonantly coupled to the cavity mode when it is in state $|0\rangle=|\uparrow\rangle$. In this case we have $\delta_{qd}=0$, and in the limit of large atomic cooperativity $|\mathcal{C}|\gg 1$, the cavity reflectivity approaches $r(\omega_c)=1$. If the QD is instead in state $|1\rangle=|\downarrow\rangle$ there is little coupling between the QD and cavity either due to selection rules $(g=0)$ or large detuning, so all of the light is transmitted through the cavity. Therefore, the qubit state of the QD will switch the cavity from being highly reflecting to highly transmitting. This operation can be viewed as a controlled-NOT gate between the state of the QD and the propagation direction of the scattered light. Controlled reflectivity of a cavity via a single QD has been reported in several works [18,26,27].

For the atom, we assume that the driving field is detuned from the resonant transition frequency ω_a by $\delta_a=\omega-\omega_a$. If the atom is in state $|0\rangle$, it will induce off-axis elastic scattering via the near resonant optical transition to state $|e\rangle$. The scattered field is collected by an objective lens and coupled into a single mode fiber. We define β as the coherent-state amplitude of the field scattered into the fiber. In contrast, when the atom is in state $|1\rangle$ it will not scatter any light since it cannot make an optical transition due to selection rules. For the case of $^{171}Yb^+$, we identify $|0\rangle$ and $|1\rangle$ states as the $F=1, m_F=1$ and $F=2, m_F=2$ hyperfine levels of the metastable electronic $^2D_{3/2}$ state (53 ms lifetime), with a frequency splitting of 0.86 GHz. With the 935 nm input laser field linearly polarized parallel to a weak magnetic field, the $|0\rangle$ state couples to the $^3[3/2]_{1/2}$ $F=1, m_F=1$ hyperfine level we identify as state $|e\rangle$, while the $|1\rangle$ state remains dark, as indicated in Fig. 1(b).

We define the input coherent field amplitude incident on the cavity mode as α_{in}. If the QD is in state $|0\rangle$ then the reflected and transmitted field amplitudes are then given by $\alpha=r(\omega)\alpha_{in}$ and $\alpha_T=t(\omega)\alpha_{in}$, respectively. If instead the QD is in state $|1\rangle$ all of the light is transmitted because the incident field is resonant with the cavity. Similarly, if the atom is in state $|0\rangle$ the scattered field is β, while if it is in state $|1\rangle$ there is no scattered field amplitude. Under the assumption that the input field to the cavity and scattered field from the atom are weak we can expand them to first order in photon number. Before the beamsplitter the atom, QD, and fields are described by the wave function

$$\psi_i = \frac{1}{2}[(1 + \alpha\hat{\mathbf{a}}^\dagger + \alpha_T\hat{\mathbf{e}}^\dagger + \beta\hat{\mathbf{b}}^\dagger)|0\rangle_{\mathrm{QD}}|0\rangle_a + (\alpha\hat{\mathbf{a}}^\dagger + \alpha_T\hat{\mathbf{e}}^\dagger) \times |0\rangle_{\mathrm{QD}}|1\rangle a + (\alpha_{in}\hat{\mathbf{e}}^\dagger + \beta\hat{\mathbf{b}}^\dagger)|1\rangle_{\mathrm{QD}}|0\rangle_a + (\alpha_{in}\hat{\mathbf{e}}^\dagger)|1\rangle_{\mathrm{QD}}|1\rangle_a] \times |\mathrm{vac}\rangle, \tag{3}$$

where $\hat{\mathbf{a}}$ and $\hat{\mathbf{e}}$ are the bosonic operator for the reflected and transmitted modes of the cavity and $\hat{\mathbf{b}}$ is the bosonic operator for the scattered mode from the atom. The state $|\mathrm{vac}\rangle$ represents the vacuum state of all field modes. The beamsplitter then applies the transformations

$$\hat{\mathbf{a}} \rightarrow \frac{\hat{\mathbf{d}}_1 + \hat{\mathbf{d}}_2}{\sqrt{2}}, \tag{4}$$

$$\hat{\mathbf{b}} \rightarrow \frac{\hat{\mathbf{d}}_1 - \hat{\mathbf{d}}_2}{\sqrt{2}}, \tag{5}$$

where $\hat{\mathbf{d}}_1$ and $\hat{\mathbf{d}}_2$ are the bosonic modes monitored by detector 1 and detector 2 respectively. Conditioned on a photon detection event at detector 2, the state of the QD and atom collapses onto

$$|\psi_f\rangle = D^{-1}[(\alpha-\beta)|0\rangle_{qd}|0\rangle_a + \alpha|1\rangle_{qd}|0\rangle_a - \beta|0\rangle_{qd}|1\rangle_a], \tag{6}$$

where $D^2=(|\alpha-\beta|^2+|\alpha|^2+|\beta|^2)$. By tuning the phase and amplitude of the input fields so that $\alpha=\beta$, the above state becomes a maximally entangled Bell state $|\psi_f\rangle=(|1\rangle_{qd}|0\rangle_a - |0\rangle_{qd}|1\rangle_a)/\sqrt{2}$. It should be noted that, so long as the quasimonochromatic limit is valid, a perfect entangled state can be generated even when the QD and atom have different resonant frequencies and decay rates.

III. FIDELITY UNDER PULSED EXCITATION

The ideal protocol described in Sec. II considers the quasimonochromatic limit, where the input pulses are sufficiently long in time to be considered as single frequency. In a real experiment, the entanglement operation must be completed before the QD and atom have had time to decohere, which requires excitation with short optical pulses. The coherence time of the atomic hyperfine states can be long, but the QD spin coherence time is much shorter (10 ns) due to hyperfine interactions with nuclear spin [28]. Recent progress in optical locking of nuclear-spin polarization suggests that much longer lifetimes in the microsecond regime may be possible [29–31]. Nevertheless, it is important to consider the effect of short pulses (0.1–10 ns) on the quality of the generated entangled state.

In order to quantify the quality of the generated entanglement we require a metric for how close the state we generate is to the desired state. The simplest choice is the fidelity, defined as $F=\langle\psi_d|\rho|\psi_d\rangle$, with $|\psi_d\rangle$ being the desired state of the system and ρ the actual density matrix. Fidelity can be interpreted as the average distance between the actual and desired state that takes on the ideal value of 1 when the two are identical, and for Bell states, a fidelity greater than 0.5 indicates entanglement. Of course other entanglement monotones exist that are independent of the form of the desired state, but they generally require complete knowledge of the actual state density matrix [32,33].

Because we consider the weak excitation regime, the cavity-QD system and trapped atom are linear scatterers.

Therefore, we may analyze the effect of time varying excitation by Fourier decomposing the time-dependent input fields and looking at the scattering behavior of each Fourier component independently. Such approach would not be valid in the strong excitation limit where nonlinear scattering occurs due to absorption saturation. We defer that discussion to Sec. VI.

In order to analyze the spectral properties of the field scattered by the atom, we need a more precise expression for its scattering amplitude. To derive this amplitude, we consider a fully quantum description of the scattering process (although a classical description of the field gives the same answer). We begin with the standard system Hamiltonian for the atom given by

$$\mathbf{H} = \sum_{\mathbf{k}} \hbar\omega_k \hat{\mathbf{b}}_{\mathbf{k}}^{\dagger}\hat{\mathbf{b}}_{\mathbf{k}} + \sum_{\mathbf{k}} \hbar\omega_k \hat{\mathbf{q}}_{\mathbf{k}}^{\dagger}\hat{\mathbf{q}}_{\mathbf{k}} + \frac{\sigma_z}{2}\omega_a + \sum_{\mathbf{k}} \hbar g_{\mathbf{k}}(\sigma_+ \hat{\mathbf{b}}_{\mathbf{k}} e^{i\mathbf{k}\cdot\mathbf{r}} + \sigma_- \hat{\mathbf{b}}_{\mathbf{k}}^{\dagger} e^{-i\mathbf{k}\cdot\mathbf{r}}) + \sum_{\mathbf{k}} \hbar g_{\mathbf{k}}(\sigma_+ \hat{\mathbf{q}}_{\mathbf{k}} e^{i\mathbf{k}\cdot\mathbf{r}} + \sigma_- \hat{\mathbf{q}}_{\mathbf{k}}^{\dagger} e^{-i\mathbf{k}\cdot\mathbf{r}}) + V_{\text{trap}}.$$

In the above equation, ω_a is the resonant frequency of the atom, σ_z is the population difference operator for atom scattering transition, and σ_+/σ_- is the transition raising/lowering operator. These operators act on the ground state which is the $^2D_{3/2}$ hyperfine $|1,1\rangle$ state, and the excited state which is the $^3[3/2]_{1/2}$ $|1,1\rangle$ state as illustrated in Fig. 1 (note that the field does not couple the $^2D_{3/2}$ hyperfine $|2,2\rangle$ state due to selection rules, so this dipole transition is not included in the Hamiltonian). The electromagnetic modes have been separated into a set of input modes corresponding to the bosonic operators $\hat{\mathbf{q}}_{\mathbf{k}}$, and a set of output modes corresponding to the bosonic operators $\hat{\mathbf{b}}_{\mathbf{k}}$. The separation of input and output modes is carried out to distinguish modes used to drive the QD from those used to collect scattered light. The scattered modes are coupled to the atomic dipole by the coupling strength $g_{\mathbf{k}}=-\hat{\mathbf{d}}\cdot\boldsymbol{\epsilon}_{\mathbf{k}}\sqrt{\omega_{\mathbf{k}}/\hbar\epsilon_0 V}$ where V is the quantization volume and $\hat{\mathbf{d}}=d\hat{\mathbf{z}}$ is the atomic dipole moment. The potential V_{trap} is the harmonic trapping potential of the atom, while $\mathbf{r}$ is the location of the atom in the trap.

We first consider the stationary atom limit, where $\mathbf{r}$ is a real vector. Atomic recoil, which requires us to account for the quantized operator nature of $\mathbf{r}$, will be addressed in the next section. When the atom is in qubit state $|0\rangle$ the Heisenberg equations of motion for the atomic and cavity field operators are given by

$$\frac{d\hat{\mathbf{b}}_{\mathbf{k}}}{dt} = -i\omega_{\mathbf{k}}\hat{\mathbf{b}}_{\mathbf{k}} - ig_{\mathbf{k}}\sigma_- e^{i\mathbf{k}\cdot\mathbf{r}}, \tag{7}$$

$$\frac{d\hat{\mathbf{q}}_{\mathbf{k}}}{dt} = -i\omega_{\mathbf{k}}\hat{\mathbf{q}}_{\mathbf{k}} - ig_{\mathbf{k}}\sigma_- e^{i\mathbf{k}\cdot\mathbf{r}}, \tag{8}$$

$$\frac{d\sigma_-}{dt} = -(i\omega_a + 1/T_2) - i\sum_{\mathbf{k}'} g_{\mathbf{k}'}\hat{\mathbf{b}}_{\mathbf{k}'} e^{i\mathbf{k}'\cdot\mathbf{r}} - i\sum_{\mathbf{k}'} g_{\mathbf{k}'}\hat{\mathbf{q}}_{\mathbf{k}'} e^{i\mathbf{k}'\cdot\mathbf{r}}, \tag{9}$$

where T_2 is the pure dephasing time of the atom. In Eq. (9) we make the weak excitation approximation that the atom remains mostly in the ground state, so $\sigma_z \to -1$ [10]. Equations (7)–(9) can be solved by direct integration to give

$$\sigma_- = -i\sum_{\mathbf{k}'} \frac{\mathcal{L}(\delta_{\mathbf{k}'}, \gamma_a)}{\gamma_a} g_{\mathbf{k}'}\hat{\mathbf{q}}_{\mathbf{k}'}(0) e^{i(\mathbf{k}'\cdot\mathbf{r} - \omega_{\mathbf{k}'}t)}, \tag{10}$$

where $\delta_{\mathbf{k}'} = \omega_a - \omega_{\mathbf{k}'}$, $\gamma_a = \gamma_r/2 + 1/T_2$, $\gamma_r = d^2\omega_a^3/3\pi\epsilon_0\hbar c^3$ is the spontaneous emission rate, and $\gamma/(i\omega+\gamma)$. In deriving the above equation we consider only the forced response of the atom driven by the input modes, and ignore the transient response due to turn-on of the input field. We omit the term associated with the initial condition of the output modes with no loss of generality because the output modes are initially in a vacuum, so their contribution vanishes when operating on the initial state. Plugging into Eq. (7) and integrating, we subsequently obtain

$$\hat{\mathbf{b}}_{\mathbf{k}} = -\pi g_{\mathbf{k}}\sum_{\mathbf{k}'} \frac{\mathcal{L}(\delta_{\mathbf{k}'}, \gamma_a)}{\gamma_a} g_{\mathbf{k}'}\hat{\mathbf{q}}_{\mathbf{k}'}(0) e^{i(\mathbf{k}'-\mathbf{k})\cdot\mathbf{r}} e^{-i\omega_{\mathbf{k}'}t}\delta(\omega_{\mathbf{k}} - \omega_{\mathbf{k}'}). \tag{11}$$

Each input mode is assumed to be initially populated with a coherent field characterized by the coherent field amplitude $q_{\mathbf{k}'}$. Because the input fields are coherent states and the atom is a linear scatterer due to the weak excitation assumption, the output fields must also be coherent states. The coherent-state amplitude of the output fields is given by

$$\langle\hat{\mathbf{b}}_{\mathbf{k}}\rangle = -\pi g_{\mathbf{k}} e^{-i\omega_{\mathbf{k}}}\sum_{\mathbf{k}'} \Omega(\mathbf{k}') e^{i(\mathbf{k}'-\mathbf{k})\cdot\mathbf{r}} \frac{\mathcal{L}(\delta_{\mathbf{k}'}, \gamma_a)}{\gamma_a}\delta(\omega_{\mathbf{k}} - \omega_{\mathbf{k}'}), \tag{12}$$

where we define the Rabi frequency $\Omega(\mathbf{k}') = g_{\mathbf{k}'}q_{\mathbf{k}'} = -dE_{\mathbf{k}'}/\hbar$, with $E_{\mathbf{k}'}$ being the electric field amplitude of the input modes. We make the assumption that the input modes are approximately collimated and propagating in the x direction of our coordinate system. Under this approximation we have $e^{i\mathbf{k}'\cdot\mathbf{r}} \approx e^{i\mathbf{k}_{\omega_{\mathbf{k}'}}\cdot\mathbf{r}}$ where $\mathbf{k}_{\omega_{\mathbf{k}'}} = \hat{\mathbf{x}}\omega_{\mathbf{k}'}/c$. Taking the quantization volume to be infinitely large, we can convert the sum to an integral. We define $\beta_{\mathbf{k}} = \langle\hat{\mathbf{b}}_{\mathbf{k}}\rangle e^{i\omega_{\mathbf{k}}}$ as the coherent-state amplitude in the rotating reference frame. This field amplitude is given by

$$\beta_{\mathbf{k}} = -\pi\frac{\mathcal{L}(\omega_a, \gamma_a)}{\gamma_a}\Omega(\omega_k) e^{i(\mathbf{k}_\omega - \mathbf{k})\cdot\mathbf{r}}, \tag{13}$$

where $\Omega(\omega_k) = -dE(\omega_{\mathbf{k}})/\hbar$ with $E(\omega_{\mathbf{k}})$ being the Fourier transform component (as opposed to the Fourier series component in the summation) of the electric field amplitude at the location of the atom. The above coherent-state amplitudes give a full quantum-mechanical description of the scattered field of the atom. In Appendix A we show that the total

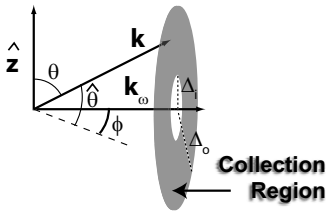

FIG. 2. Model for collection optics. All k vectors between the angles Δ_i and Δ_o from the input propagation direction (shaded region) are collected by the fiber. All other k vectors are not collected

number of scattered photons $N_s=\Sigma_{\mathbf{k}}|\beta_k|^2$ is given by

$$N_s = |\mathcal{L}(\omega_a,\gamma_a)|^2\left(\frac{\gamma_r}{\gamma_a}\right)^2\sigma_0 n_i, \tag{14}$$

where ω_0 is the center frequency of the incident field, n_i is the input photon flux density given by $n_i=I/\hbar\omega_0$, where I is the input field intensity, γ_r is the radiative decay rate of the atom to state $|0\rangle$, and $\sigma_0=3\lambda^2/2\pi$ is the atomic cross section.

The important quantity for our analysis is $\beta(\omega)$, the amplitude of the coherent field coupled to the fiber at frequency ω. Since the collection optics are comprised of only linear optical elements, the fiber amplitude $\beta(\omega)$ is related to the free-space scattered amplitudes $\beta_{\mathbf{k}}$ by the linear transformation

$$\beta(\omega) = \sum_{|\mathbf{k}|=\omega/c} s_{\mathbf{k}}\beta_{\mathbf{k}}, \tag{15}$$

where $s_{\mathbf{k}}$ are a set of complex scattering coefficients representing a unitary transformation. To proceed, we need a model for the collection optics. Here we consider a simple model, illustrated in Fig. 2, where all k vectors between a solid angle Δ_i and Δ_o (taken with respect to the propagation direction of the pump) are collected by the fiber. The remaining k vectors do not couple to the fiber. Thus, $s_{\mathbf{k}}=s$ if $\mathbf{k}$ is within the collection window, and $s_{\mathbf{k}}=0$ if $\mathbf{k}$ is outside the collected solid angle. The omission of solid angles between 0 and Δ_i is included in order to reject the input beam. For a well collimated input, we can take the limit that $\Delta_i\to 0$. The simple model we consider captures all of the relevant physics, and provides good numerical accuracy for our calculations. A more accurate model would treat $s_{\mathbf{k}}$ as a Gaussian transverse distribution, matching the Gaussian profile of the single mode fiber. This model would significantly complicate the calculations but would ultimately yield similar results.

Our calculations focus on the *paraxial limit*, where the collected solid angle Δ_o is small, so that the collected light propagates nearly parallel to the input beam. We focus on this range of collection angles because it is known to minimize the effect of atomic recoil [22,23], as we will analyze in more detail in the next section. Using the simple model for the collection optics, we shown in Appendix B that in the paraxial limit

$$\beta(\omega) = \beta_0\mathcal{L}(\delta_a,\gamma_a)\Omega(\omega) \tag{16}$$

with

$$\beta_0 = \frac{d\omega_0^{3/2}}{2c\gamma_a\sqrt{2\epsilon_0\hbar L_x A}}\int_A d\theta d\phi e^{ik_0(\hat{\mathbf{x}}-\hat{\mathbf{k}})\cdot\mathbf{r}}. \tag{17}$$

In the above equation the integral is taken over the collection area, while $A=2\pi(\cos\Delta_i-\cos\Delta_o)\approx\pi(\Delta_o^2-\Delta_i^2)$ is the area that the collection region occupies on the unit sphere and L_x is the length of the quantization volume in the x direction. For simplicity we assume that ω_k can be replaced by its average value ω_0 and $k_0=\omega_0/c$. We do not make this substitution in the Lorentzian function, however, because near resonance this function will vary rapidly even over a narrow bandwidth of interest.

In the monochromatic limit, we could always achieve the matching condition $\alpha=\beta$ by changing the amplitude and phase of the incident fields. But under pulsed excitation, the reflection coefficient of the QD-cavity system has a spectral profile described by Eq. (2), while the atom scattering amplitude follows primarily a Lorentzian profile. Thus, each spectral component will require a different matching condition. Since we cannot satisfy the matching condition perfectly for each frequency we expect that the generated state will no longer be perfectly entangled. It has previously been shown that the spectral width over which high reflection is achieved when a QD is coupled to a cavity is given by the inverse modified spontaneous emission lifetime of the cavity enhanced QD transition [10], typically 10–50 GHz. This bandwidth represents a response time which is much faster than any decay rates of the atom. Thus, we expect the fidelity of the generated entangled state to be dominated by the dispersive properties of the atom, which are much narrower in frequency than those of the QD.

To calculate the fidelity of the generated entangled state under pulsed excitation, we begin with the state of the system after the field from the QD-cavity system is mixed with the scattered field from the atom on the beamsplitter, as shown in Fig. 1. We once again assume that the scattered fields are sufficiently weak so that they may be expanded to first order in photon number. After the beamsplitter the state of the fields, atom and QD can be written as

$$|\psi_f\rangle = \int d\omega\frac{1}{2\sqrt{2}}\Bigg[\int[\alpha(\omega)-\beta(\omega)]|00\rangle + \alpha(\omega)|01\rangle-\beta(\omega)|10\rangle\Bigg]\hat{\mathbf{v}}_\omega^\dagger|\text{vac}\rangle+|f\rangle. \tag{18}$$

In the above state the operator $\hat{\mathbf{v}}_\omega$ is the bosonic operator for a photon in the mode detected by detector 2, and state $|f\rangle$ is an un-normalized state representing the remaining components of the wave function that do not contain any photons in the detection mode. From the expressions for the reflection coefficients we have

$$\alpha(\omega) = \alpha_0 r(\omega)\Omega(\omega), \tag{19}$$

$$\beta(\omega) = \beta_0\mathcal{L}(\delta_a,\gamma_a)\Omega(\omega), \tag{20}$$

where α_0 and β_0 are complex amplitudes that can be adjusted by selecting the amplitude and phase of the input pulse. In the ideal case we would have $\alpha(\omega)=\beta(\omega)$ for all frequencies,

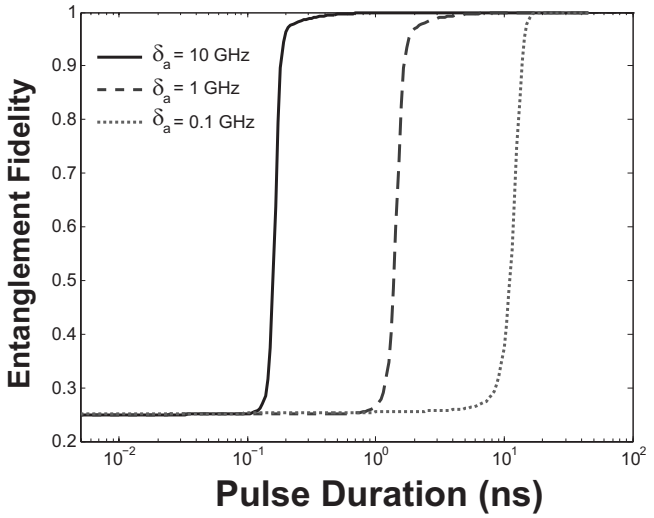

FIG. 3. Entanglement fidelity as a function of pulse duration for several different values of atomic detuning $\delta_a=\omega-\omega_a$. For each detuning, there is a certain value of the pulse duration where the fidelity quickly drops from 1 (ideal entangled state) to 0.25 (no coherence between α and β). Larger δ_a enables shorter pulses before fidelity drops.

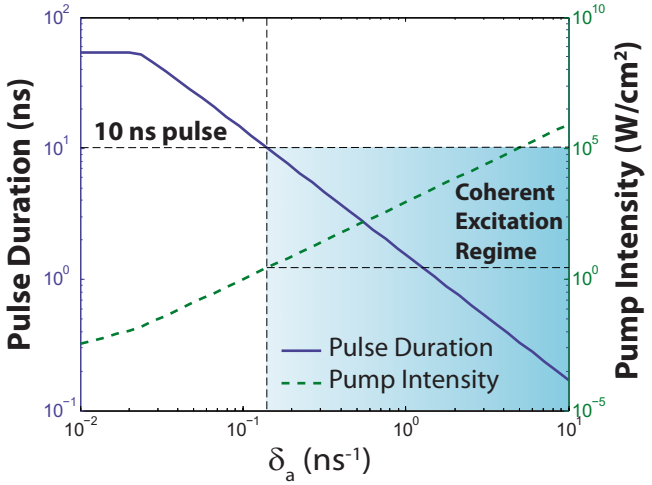

FIG. 4. (Color online) Solid line plots pulse duration required to achieve fidelity of 0.9 as a function of δ_a. Dashed line plots pump intensity required to achieve 0.1 scattered photons in the pulse. As $\Delta\omega_a$ increases, we can use shorter pulses but require higher excitation energies to achieve the same scattering rate. If the coherence time of the QD is 10 ns, the shaded region represents the parameter regime where entanglement can be achieved.

which would reproduce the ideal fidelity of the monochromatic limit. Unfortunately, dispersion prohibits us from achieving this for all values of ω. The best we can do is adjust the amplitudes so that $\alpha(\omega_0)=\beta(\omega_0)$, where ω_0 is the center frequency of the pulse.

The fidelity of the entangled state can be determined by first calculating the reduced density matrix of the QD-atom system conditioned on a detection event at detector 2. This reduced density matrix is given by

$$\rho=\frac{\mathrm{Tr}_{\mathrm{fields}}\{\mathbf{P}|\psi_f\rangle\langle\psi_f|\}}{\mathrm{Tr}\{\mathbf{P}|\psi_f\rangle\langle\psi_f|\}}, \tag{21}$$

where $\mathbf{P}$ is a projector onto the subspace containing at least one photon in the detection mode for detector 2. The fidelity can be calculated using $F=\langle\psi_-|\rho|\psi_-\rangle$, where $|\psi_-\rangle$ is the ideal spin singlet entangled state. The expression for fidelity is given by

$$F=\frac{1}{4}\frac{\int d\omega|\alpha(\omega)+\beta(\omega)|^2}{\int d\omega|\alpha(\omega)|^2+|\beta(\omega)|^2-\mathrm{Re}\{\alpha(\omega)\beta(\omega)\}}. \tag{22}$$

Figure 3 plots the fidelity as a function of the pulse duration of the external field for several values of the detuning from atomic resonance. The curves are obtained by numerical integration of Eq. (22). We assume the input pulse is Gaussian with a spectrum given by $\Omega(\omega)=\Omega_0 e^{-\tau^2(\omega-\omega_0)^2/4}e^{i(\mathbf{k}\cdot\mathbf{r}-\omega t)}$, where τ is the pulse duration. To calculate the reflection coefficient for the cavity containing the QD we use parameters that are appropriate for InAs QDs coupled to photonic crystal defect cavities. Using experimental values from recent work [26], we set $g/2\pi=16$ GHz, $\delta_{qd}=0$, $\kappa/2\pi=25$ GHz, and $\gamma_{qd}/2^*\pi=160$ MHz. For the $^{171}\mathrm{Yb}^+$ atomic ion we use $\gamma_a/2\pi=4.2$ MHz, the linewidth of the $^3[3/2]_{1/2}$ state.

In the long pulse limit, the fidelity approaches its ideal value for all atomic detunings. However, for each value of atomic detuning the fidelity makes a rapid transition from $F=1$ to $F=0.25$ at some critical pulse duration. Thus, the range of pulses for which the monochromatic approximation is valid will depend on δ_a. At detuning of $\delta_a=0.1$ GHz, the transition occurs roughly at 10 ns pulse duration, which is on the order of the coherence time of the QD. By increasing the detuning to 1 GHz, the fidelity transitions at 1 ns pulse duration, well below the QD decoherence time. By further increasing the detuning to 10 GHz it is possible to use 100 ps pulses. Thus, by increasing the atomic detuning we can use shorter pulses to achieve high fidelity. This tradeoff occurs because the dispersion, dominated by a Lorentzian function, is maximum near resonance and tails off with larger detuning.

The disadvantage of going to larger detuning is that we need to use more pump power in order to achieve the same scattering rate. The number of scattered photons is given by Eq. (14). From this equation one can see that as δ_a increases the Lorentzian decays in amplitude, forcing us to increase the incident photon density n_i to attain the same number of scattered photons. The tradeoff between pulse duration and pump intensity is shown in Fig. 4. The panel plots both the pulse duration required to achieve a fidelity of 0.9 (solid blue curve) and the pump intensity required to scatter $N_s=0.1$ photons (dashed green curve) as a function of δ_a. The choice of $N_s=0.1$ ensures that the collected field is sufficiently weak to be expanded to first order in photon number. The shaded area, labeled the *coherent excitation regime*, represents the operating region where the pulse duration is less than 10 ns, the typical dephasing time of the InAs QD electron spin [34]. The coherence time of the atom is expected to be longer, so the QD limits the coherence time of the overall entangled state. One can see from the figure that pump intensities as

low as 2 W/cm^2 would be sufficient to enable the use of 10 ns pulses with the specified scattering rate.

IV. DECOHERENCE DUE TO ATOM RECOIL

Entanglement between the atom and QD relies on the assumption one cannot distinguish whether a photon was reflected from the cavity or scattered from the atom, even in principle. Atomic recoil can serve to betray this which-path information [22,23]. When the atom scatters a photon there is a probability that it will recoil, leaving residual kinetic energy in the motional degrees of freedom of the center-of-mass wave function. To achieve high fidelity we require that this recoil probability is small. In this section we analyze recoil in the monochromatic field limit. Later, we will extend this analysis to pulsed input.

Atomic recoil is already present in the expression for the scattered field amplitude given in Eqs. (16) and (17). Previously we assumed that the position $\mathbf{r}$ of the atom was fixed, and therefore the integral term in the expression was simply a complex constant. To include the effect of recoil, we must treat $\mathbf{r}$ as the position operator and trace over the motional degrees of freedom of the atom. We define the initial state of the atom-QD system by the density matrix

$$\rho_i = \sum_n p(n)|\psi_{ni}\rangle\langle\psi_{ni}|, \tag{23}$$

where

$$|\psi_{ni}\rangle = \frac{1}{2}(|00\rangle + |11\rangle + |10\rangle + |01\rangle)|n\rangle|\text{vac}\rangle. \tag{24}$$

In the above equations, $|n\rangle$ is the harmonic-oscillator eigenstate for the center-of-mass motion of the atom, $|\text{vac}\rangle$ is the vacuum field for all optical modes, and $p(n)$ is assumed to be a thermal distribution. After interaction with the two input fields, the state in Eq. (24) is transformed into

$$|\psi_{nf}\rangle = |\psi_d\rangle|n\rangle|v\rangle + |f_n\rangle \tag{25}$$

with

$$|\psi_d\rangle = \frac{1}{2}\left[\left(\frac{\alpha-\beta}{\sqrt{2}}\right)|00\rangle + \frac{\alpha}{\sqrt{2}}|01\rangle - \frac{\beta}{\sqrt{2}}|10\rangle\right]. \tag{26}$$

The state $|v\rangle$ represents a single photon in the detection mode that is monitored by detector 2, while $|f_n\rangle$ is once again a wave function orthogonal to $|v\rangle$ representing the state of the QD, atom, and all fields when there are no photons in mode $\hat{\mathbf{v}}$. Conditioned on a detection event at detector 2, the final density matrix of the system is given by

$$\rho_f = \frac{\text{Tr}_n\left\{\mathbf{P}\sum_n p(n)|\psi_{nf}\rangle\langle\psi_{nf}|\right\}}{\text{Tr}\left\{\mathbf{P}\sum_n p(n)|\psi_{nf}\rangle\langle\psi_{nf}|\right\}}, \tag{27}$$

where Tr_n represents a trace over all degrees of freedom except for the qubit states of the atom and QD, and $\mathbf{P} = |v\rangle\langle v|$ is once again a projection operator that projects on the subspace containing one photon in the photon mode monitored by detector 2.

The fidelity F of the final state can be defined as the overlap between the actual state of the system and the desired state $|\psi_-\rangle = (|01\rangle - |10\rangle)/\sqrt{2}$. Thus,

$$F = \langle\psi_-|\rho_f|\psi_-\rangle. \tag{28}$$

Using the definition of ρ_f in Eq. (27) we attain the following expression for the fidelity:

$$F = \frac{1}{4}\frac{|\alpha|^2 + \langle|\beta|^2\rangle + 2\alpha\,\text{Re}\{\langle\beta\rangle\}}{|\alpha|^2 + \langle|\beta|^2\rangle - \alpha\,\text{Re}\{\langle\beta\rangle\}}, \tag{29}$$

where

$$\langle\beta\rangle = \sum_n p(n)\langle n|\beta|n\rangle, \tag{30}$$

$$\langle|\beta|^2\rangle = \sum_n p(n)\langle n||\beta|^2|n\rangle. \tag{31}$$

The expressions in Eqs. (30) and (31) can be evaluated under the assumption that the atom occupies a thermal distribution. In this case, we can then write [22,23,35,36]

$$\langle e^{i(\mathbf{k}_\omega - \mathbf{k})\cdot\mathbf{r}}\rangle = e^{-\eta^2(1-\cos\hat{\theta}\cos\phi)(\bar{n}+1/2)}, \tag{32}$$

where $\bar{n}$ is the average excitation number of the atom in the harmonic potential, and $\eta = k\sqrt{\hbar/2m_{\text{atom}}\omega_t}$ with m_{atom} being the mass of the atom and ω_t the trap frequency. The dimensionless constant η is called the Lamb-Dicke parameter and determines the extent to which an atom will recoil. Since we are primarily interested in small angles $\hat{\theta}$ and ϕ, we expand the cosine terms in the exponent to second order in these angles. Using this approximation, we show in Appendix C that

$$\langle\beta\rangle = -\sqrt{\langle|\beta|^2\rangle}\frac{1-\exp[-\eta^2(\bar{n}+1)\Delta^2]}{\eta^2(\bar{n}+1)\Delta^2}, \tag{33}$$

$$\langle|\beta|^2\rangle = \frac{3}{8}N_s\Delta^2. \tag{34}$$

The above expression is derived in the limit that $\Delta_i \to 0$ and $\Delta_o = \Delta$. The matching condition $\alpha = \beta$ cannot be satisfied because β now fluctuates due to recoil. The fidelity is maximized when $\alpha = -\sqrt{\langle|\beta|^2\rangle}$ which indicates that α is set to the average amplitude of β and has the same phase. Under this optimal condition, the fidelity is given by

$$F = \frac{1+f(\Delta)}{4-2f(\Delta)}, \tag{35}$$

where

$$f(\Delta) = \frac{1-\exp[-\eta^2(\bar{n}+1)\Delta^2]}{\eta^2(\bar{n}+1)\Delta^2}. \tag{36}$$

The function $f(\Delta)$ determines the extent to which recoil degrades the fidelity of the entangled state. When $\eta^2(\bar{n}+1)\Delta^2 \ll 1$ then $f(\Delta) \to 1$ and the state takes on the ideal entanglement fidelity of 1. In the opposite limit $[\eta^2(\bar{n}+1)\Delta^2$

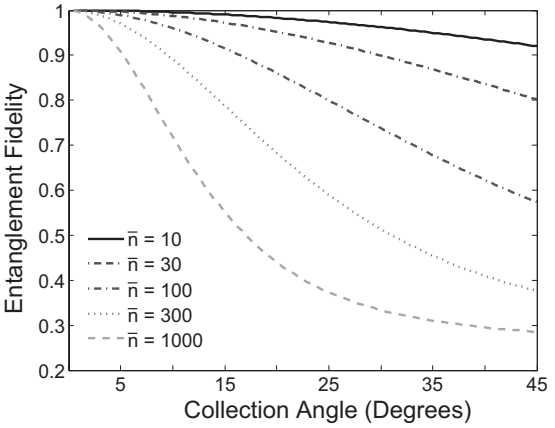

FIG. 5. Entanglement fidelity as a function of collection angle for the atom emission with various atom thermal states, characterized by the average vibrational occupation number $\bar{n}$.

$\gg 1]f(\Delta)\to 0$ and the fidelity is degraded to $F=1/4$, which is the fidelity attained when the atom scatters an incoherent field. Equation (35) allows us to calculate the fidelity of the entangled state in the monochromatic limit as a function of the atom temperature ($\bar{n}$) and the collection angle.

Figure 5 plots the entanglement fidelity as a function of collected solid angle for different values of $\bar{n}$. Calculations were performed for a 1 MHz trap frequency, using the emission frequency of 935nm and the mass of $^{171}Yb^{+}$. For these numbers, the Lambe-Dicke parameter is given by $\eta=0.09$, which means that the atom is in the Lamb-Dicke regime for $\bar{n}<11.1$. One can see from Fig. 5 that for $\bar{n}=10$, the fidelity is greater than 0.9 even for large collection angles. For higher trap temperatures there is a tradeoff between the fidelity and the collection angle.

V. PHOTONIC LEAKAGE OF WHICH-PATH INFORMATION

The tradeoff between fidelity and collection angle implies that there will be a tradeoff between fidelity and entanglement success probability, because larger collection angle results in higher collection efficiency of scattered photons. We define the entanglement success probability as the probability that detector 2 registers a photon count. This probability is given by

$$P_{\text{success}}=\text{Tr}\left\{\mathbf{P}\sum_{n}p(n)|\psi_{nf}\rangle\langle\psi_{nf}|\right\}, \tag{37}$$

where $|\psi_{nf}\rangle$ is defined in Eq. (25). Inserting this definition into the above equation we obtain

$$P_{\text{success}}=\frac{1}{4}(|\alpha|^2+\langle|\beta|^2\rangle-\text{Re}\{\alpha\langle\beta\rangle\}). \tag{38}$$

Since the optimal fidelity is always achieved when the amplitudes of the interferometer are matched such that $|\alpha|^2=\langle|\beta|^2\rangle$, we can then use Eqs. (33) and (34) to write

$$P_{\text{success}}=\frac{3N_s\Delta^2}{32}[2-f(\Delta)], \tag{39}$$

where $f(\Delta)$ is defined in Eq. (36). In the high fidelity limit $f(\Delta)\approx 1$ and we have

$$P_{\text{success}}=3N_s\Delta^2/32. \tag{40}$$

Note that decoherence due to recoil increases the success probability. This increase is due to "bad" detection events when the QD and atom are both in the 0 qubit states, which would destructively interfere under ideal conditions.

To investigate the entanglement success probability we need to determine how large we can make N_s. The expression for fidelity in Eq. (35) does not depend on N_s because it was derived under the assumption that the scattered field is sufficiently weak so that it could be expanded to first order in photon number. If we make N_s too large this assumption will no longer be valid. Thus, we need to derive a more precise expression for the fidelity that accounts for both recoil and the probability that more than one photon is scattered by the atom.

If the atom scatters more than one photon, this can lead to leakage of which-path information. This information leakage can be understood from the following simple argument. First, we note that in general the collection efficiency of scattered light is small. Even with a collected solid angle of 45°, which corresponds to a numerical aperture of 1, only 20% of the photons are collected into the fiber. Reflection and absorption losses from the optics will serve to degrade this collection efficiency even more. If the atom scatters two photons it is much more likely that only one of the photons is collected than it is that both photons are collected. The photon which fails to be collected is never mixed on the beamsplitter, and therefore retains the information that the atom caused a scattering event causing the entanglement to decohere. Thus, in order to achieve high fidelity entanglement the probability of scattering two photons must remain low.

To analyze multiphoton scattering we retain the amplitude of the field scattered by the atom to all orders in photon number, but expand the field collected into the fiber to first order in photon number. This approximation is valid because, as noted previously, fiber collection efficiency is small in the limit we consider so even if the atom scatters many photons the probability that more than one of them is collected into the fiber is still small. After the atom scatters the input field the state of the system becomes

$$|\psi_{ni}\rangle=[(1+\alpha\hat{\mathbf{a}}^{\dagger})(1+\beta\hat{\mathbf{b}}^{\dagger})|00\rangle|\chi\rangle+|11\rangle|0\rangle+(1+\alpha\dagger)|01\rangle|0\rangle+(1+\beta\hat{\mathbf{b}}^{\dagger})|10\rangle|\chi\rangle]|n\rangle. \tag{41}$$

In the above equation the state $|00\rangle|\chi\rangle$ denotes the atom and the QD are both in qubit state $|0\rangle$, and $\chi=-\sqrt{N_s(1-3\Delta^2/8)}$ is the coherent-state amplitude of the uncollected field. Because we consider only small collection efficiency $\chi\approx-\sqrt{N_s}$. Other states are defined analogously, and state $|n\rangle$ is once again the harmonic-oscillator state of the atom center of mass. Following the same procedure as in Sec. IV, the fidelity can be obtained by tracing over both the field and atom center-of-mass motion to obtain

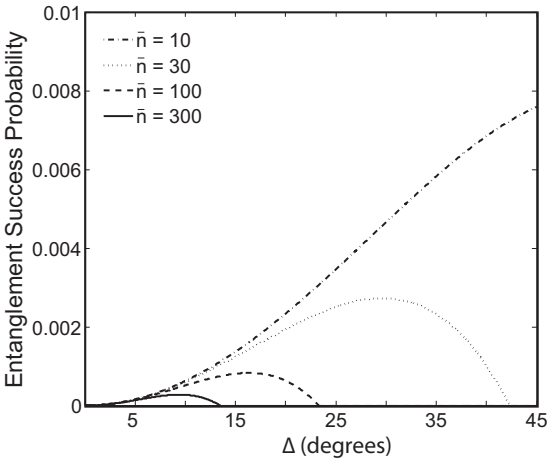

FIG. 6. Success probability for creating entanglement as a function of collection angle. The fidelity is fixed at $F=0.9$.

$$F = \frac{1 + e^{-N_s/2} f(\Delta)}{4 - 2f(\Delta)}. \tag{42}$$

The above equation gives the entanglement fidelity due to both recoil and multiphoton scattering in the monochromatic limit. One can see the interference term is degraded by $e^{-N_s/2}$, which means that to achieve high fidelity we need $N_s \ll 1$. The number of photons collected into the fiber will be subsequently much smaller, which highlights the need for efficient collection of photons.

For a fixed fidelity F, Eq. (42) gives a relationship between the scattered photon number N_s and the collected solid angle Δ. Thus, the entanglement success probability given in Eq. (40) becomes a function only of Δ. Figure 6 plots P_{success} as a function of Δ for several different trap temperatures with the same atom trap parameters used in Sec. IV, where the entanglement fidelity is held fixed at $F=0.9$. For average vibrational indices greater than $\bar{n}=10$, an optimal rate exists for a specific collection angle Δ. This optimal rate is determined by a balance between recoil and photon collection efficiency. For $\bar{n}=10$ the atom is deep within the Lamb-Dicke limit regime where fidelity is largely insensitive to recoil, so the entanglement rate is limited only by the fraction of light that can be collected by the optics.

Figure 7 plots the optimal efficiency as a function of $\bar{n}$. The efficiency is optimized with respect to the collection angle for each point, with the additional constraint that Δ cannot exceed 45°. For cold states of atomic motion within the Lamb-Dicke regime ($\bar{n}<11.1$), the efficiency is independent of $\bar{n}$. As the atomic motion leaves the Lamb-Dicke regime, the collection angle must be reduced to maintain the desired fidelity, leading to a lower success probability. In a trap with frequency $\omega_t/2\pi > 1$ MHz for an atomic $^{171}Yb^+$ ion, Doppler cooling is expected to result in a mean thermal vibrational index of $\bar{n}<10$, where success probabilities can be greater than 1%. If we use a 10 MHz experimental repetition rate, this would result in greater than 10^5 successful entanglement operations per second. Additional losses to reflection from optics and imperfect fiber coupling would serve to reduce this number.

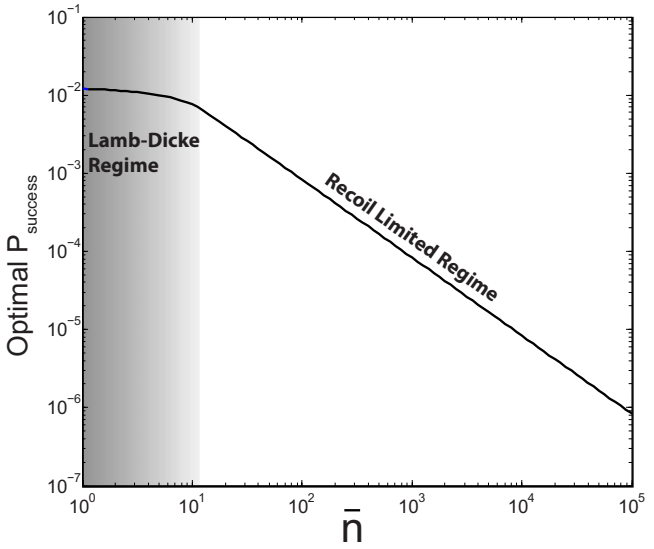

FIG. 7. (Color online) Optimum collection efficiency as a function of the average thermal vibration index of the trapped ion. The efficiency is optimized with respect to collection angle at each point, with fidelity fixed at $F=0.9$. The collection angle is restricted to not exceed 45°. The shaded area represents the regime where efficiency is limited by the collection angle of the optics. Unshaded region represents regime where efficiency is limited by recoil, and thus decreases as the ion gets hotter.

The expression derived in Eq. (42) accounts for decoherence due to both atomic recoil and multiphoton scattering. However, it is only valid in the monochromatic field limit. One can extend the analysis to the case of a pulsed field using the approach outlined in Sec. III. Since the atom and the cavity-QD system are linear scatterers in the weak excitation limit, we can decompose the pulsed input into a comb of monochromatic fields and treat each component independently. Each frequency component ω_i of the input field will create a scattered field χ_i. After mixing with the beamsplitter the final state of the QD, atom, and fields is given by

$$|\psi_{fn}\rangle = \sum_{\omega_i} \left[\frac{\alpha_i - \beta_i}{\sqrt{2}} |00\rangle + \frac{1}{\sqrt{2}} (\alpha_i |01\rangle |\text{vac}\rangle - \beta_i \Pi_i |\chi_i\rangle) \right] \times |v_w\rangle |n\rangle + |f\rangle. \tag{43}$$

In the above equation, α_i and β_i are the reflected and scattered field for the ith frequency component of the input field, $|\text{vac}\rangle$ is the vacuum state of all scattered modes, $|v_w\rangle$ is the state where there is one photon in the mode monitored by detector 2, and $|f\rangle$ represents all other states where there is no photon in the detected mode. The fidelity can be determined by plugging into Eq. (27) which leads to

$$F = \frac{1}{4} \frac{\sum_{\omega_i} |\alpha_i|^2 + \langle |\beta_i|^2 \rangle + 2e^{-N_s/2} \text{Re}\{\alpha_i \langle \beta_i \rangle\}}{\sum_{\omega_i} |\alpha_i|^2 + \langle |\beta_i|^2 \rangle - \text{Re}\{\alpha_i \langle \beta_i \rangle\}}. \tag{44}$$

where N_s is the total number of photons scattered to all modes. The above equation represents a comprehensive calculation of fidelity which accounts simultaneously for recoil,

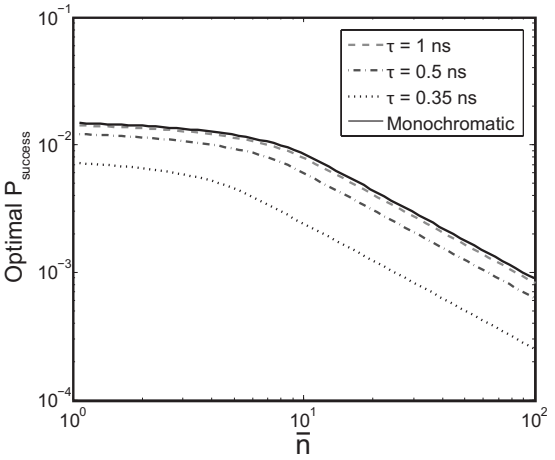

FIG. 8. Optimum collection efficiency under pulsed excitation for different pulse durations τ. The center frequency of the atomic resonance is given by $\delta_a=10$ GHz.

multiphoton scattering, and dispersion under pulsed excitation.

To perform numerical calculations we once again assume the input pulse is Gaussian with a spectrum given by $\Omega(\omega)=\Omega_0 e^{-\tau^2(\omega-\omega_0)^2/4}e^{i(\mathbf{k}\cdot\mathbf{r}-\omega t)}$, where τ is the pulse duration. Using the same parameters from Sec. III, we set the fidelity to be 0.9, which automatically creates a one-to-one relationship between N_s and Δ through Eq. (45). We then optimize P_{success} as a function of Δ, which once again is restricted not to exceed 45°, to obtain the optimal success probability as a function of $\bar{n}$. The center frequency of the input pulse is assumed to be detuned from the atomic resonance by $\delta_a=10$ GHz. The results of the calculation are shown in Fig. 8. The figure plots the optimal success probability as a function of $\bar{n}$ for pulse durations of 1, 0.5, and 0.35 ns. The calculation in the monochromatic limit is also plotted for comparison purposes. One can see that the 1 ns and 0.5 ns pulsed excitations provide performance that is very close to the monochromatic limit. For the 0.35 ns pulse there is a degradation in the success probability because dispersion reduces the base fidelity, requiring less multiphoton events in order to achieve a fidelity of 0.9. Below 0.35 ns the success probability quickly drops to zero because dispersion prevents the fidelity from achieving a value of 0.9. This reinforces the results shown in Fig. 3, which indicates that the monochromatic limit is a good approximation up until some minimum pulse duration, below which dispersion quickly degrades the fidelity.

VI. VALIDITY OF WEAK EXCITATION LIMIT

In addition to multiphoton scattering, we must also consider the validity of the weak excitation approximation. All of our calculations so far assumed that the atom and cavity-QD system are driven with sufficiently weak excitation such that $\sigma_z \rightarrow -1$, where σ_z is the population inversion operator. For the QD, it has been previously shown that the weak excitation limit is valid so long as $N_{ref}/\tau_p \ll 1/\tau_{mod}$, where N_{ref} is the number of photons reflected from the cavity, τ_p is the input pulse duration, and τ_{mod} is the modified spontaneous emission lifetime of the QD [11]. For any N_{ref} one can in principle satisfy weak excitation by make τ_p sufficiently long. It should also be noted that from the matching condition $\alpha=\beta$ and the condition that $N_s \ll 1$ (due to multiphoton scattering) we know that $N_{ref} \ll 1$. In addition, for the input pulse spectrum to fit within the high-reflection window given in Eq. (2), $\tau_p > \tau_{mod}$ [10]. When these two conditions are combined they automatically guarantee that weak excitation is satisfied for the QD. Thus, for the QD weak excitation does not impose any additional constraints on the entanglement success probability and can be generally satisfied by using sufficiently long input pulses.

We now derive a similar result for the atom. We use Eq. (10) to show that

$$\langle \sigma_+ \sigma_- \rangle = \frac{|L(\omega_0)|^2}{\gamma^2}|\Omega(\mathbf{r},t)|^2, \tag{45}$$

where $\Omega(\mathbf{r},t)=dE(\mathbf{r},t)/\hbar$. The weak excitation approximation is valid so long as $\langle \sigma_+ \sigma_- \rangle \ll 1$. This condition can be recast into a more recognizable form. The easiest way to do this is to assume that the input optical pulse is a square pulse of duration τ starting at $t=0$, with electric field amplitude E. Thus

$$\int_0^\infty |E(\mathbf{r},t)|^2 dt = |E|^2\tau = \frac{n\hbar\omega_0}{c\epsilon_0}, \tag{46}$$

where the last equality comes from Poynting's theorem. Equation (45) becomes

$$\frac{n\sigma_0|L(\omega_0)|^2\left(\frac{\gamma_r}{\gamma}\right)^2}{\tau} = \frac{N_s}{\tau} \ll \gamma. \tag{47}$$

We attain a condition for the atom which states that the rate of scattered photons should be small compared to the atom decay rate. Although this condition was attained using the assumption of a square pulse, we expect this relation to hold for most pulse shapes.

As was the case for the QD, the limitations imposed by weak excitation restrict only the rate of emitted photons, not on total photon number. In this way, weak excitation provides a weaker restriction than multiphoton scattering, and can in general be well satisfied by picking sufficiently long pulses. In a practical experiment the clock cycle for generating entanglement will almost always be long compared to the atom decay rate. This ensures that all transients have decayed between consecutive cycles of the experiment. If we combine this requirement with the restriction placed by multiphoton scattering that $N_s \ll 1$, then Eq. (47) is automatically satisfied. Thus, at the point where nonlinearities become important the system will already have decohered due to multiphoton scattering.

VII. CONCLUSION

We conclude that it appears feasible to entangle a QD and an atom by weakly scattering light from each system and

interfering these fields to produce an appropriate single-photon detection event that heralds the entanglement. Differential dispersion, atom recoil, and the multiphoton scattering can all be managed by properly selecting the input pulse duration, collected solid angle, and input pump power. It is noted that to implement the proposed protocol it is necessary to overcome difficult experimental challenges. For example, the protocol requires phase locking of all optical pulses for qubit rotation of both atom and QD, which will require pulling all optical pulses from a common laser source or using multiple phase-locked lasers, adding to the experimental difficulty. In addition, decay of the atomic $^{171}Yb^{+}$ to other transitions will require periodic re-pumping into the $^{2}D_{3/2}$ manifold. Nevertheless, the work we present suggests that entanglement between an atomic and semiconductor system is within the reach of presently available technological capabilities.

ACKNOWLEDGMENTS

This work is supported by the Intelligence Advanced Research Projects Activity (IARPA) under Army Research Office contract, the NSF Physics at the Information Frontier Program, the NSF Physics Frontier Center at JQI, and an Army Research Office Young Investigator Grant.

APPENDIX A: CALCULATION OF TOTAL SCATTERED PHOTON NUMBER

The average number of scattered photons can be calculated by $N=\Sigma_{\mathbf{k}}\langle\hat{\mathbf{b}}_{\mathbf{k}}^{\dagger}\hat{\mathbf{b}}_{\mathbf{k}}\rangle=\Sigma_k|\beta_{\mathbf{k}}|^2$. Plugging Eq. (13) into this expression we obtain

$$N=\sum_{\mathbf{k}}\pi^2\frac{g_{\mathbf{k}}^2|L(\omega_0)|^2}{\gamma^2}\Omega(\omega_{\mathbf{k}})e^{i(\mathbf{k}_\omega-\mathbf{k})\cdot\mathbf{r}}, \tag{A1}$$

$$\rightarrow\frac{V}{2\pi c}\int_0^{2\pi}d\phi\int_0^{\pi}d\theta\int d\omega\omega^2 \times\sin\theta\pi^2\frac{g_{\mathbf{k}}^2|L(\omega_0)|^2}{\gamma^2}\Omega(\omega_{\mathbf{k}})e^{i(\mathbf{k}_\omega-\mathbf{k})\cdot\mathbf{r}}, \tag{A2}$$

$$=\frac{|L(\omega_0)|^2}{\gamma^2}\frac{d^4\omega_0^3}{6\hbar^3\epsilon_0c^3}\int_{-\infty}^{\infty}d\omega|E(\omega)|^2. \tag{A3}$$

The amount of energy in the pump beam can be determines using Poynting's theorem,

$$W=\int_0^{\infty}dt\oint\frac{\mathbf{E}\times\mathbf{B}}{\mu_0}\cdot d\hat{\mathbf{a}}=\frac{A}{c\mu_0}\int_0^{\infty}E^2(t)dt,$$

where A is the cross sectional area of the pump beam. Using the definition

$$E(t)=\int d\omega E(\omega)e^{-i\omega t}, \tag{A4}$$

we attain

$$W=A\pi c\epsilon_0\int d\omega|E(\omega)|^2=N_i\hbar\omega_0 \tag{A5}$$

where N_i is the total number of photons in the pump and ω_0 is the center frequency of the quasimonochromatic pump beam. Defining the photon density $n_i=N_i/A$ we then have

$$\int d\omega|E(\omega)|^2=\frac{\hbar\omega_0n_i}{\pi c\epsilon_0}. \tag{A6}$$

Plugging this expression back into Eq. (A3), and using

$$\gamma_r=\frac{\omega_0^3d^2}{6\pi\epsilon_0\hbar c^3} \tag{A7}$$

leads directly to Eq. (14).

APPENDIX B: FIELD AMPLITUDE COLLECTED INTO OPTICAL FIBER

For each frequency ω we define a fiber mode $\mathbf{b}_\omega$. We assume the fiber is single mode so that the fiber modes are only a function of frequency (or alternately longitudinal momentum). The collection lens and fiber are linear optical components, which means that the fiber mode is related to the free-space modes by the linear transformation

$$\mathbf{b}_\omega=\sum_{k=\omega/c}s_{\mathbf{k}}\hat{\mathbf{b}}_{\mathbf{k}}. \tag{B1}$$

The sum is carried out over all free-space modes that have the same energy as the fiber mode due to linearity. Unitarity requires that

$$\sum_{k=\omega/c}|s_{\mathbf{k}}|^2=1. \tag{B2}$$

We define $\Delta\theta$ as the angle between the $\mathbf{k}$ and the input field propagation direction which is assumed to be along the x axis. We adopt a simplified model that the collection optics collect all k vectors satisfying $\Delta_i<\Delta\theta<\Delta_o$. Thus, for k-vectors satisfying this condition $s_{\mathbf{k}}=C$, where C is a constant, while $s_{\mathbf{k}}=0$ for all other k vectors.

The constant C must be determined from the condition Eq. (B2), which results in

$$\sum_{k=\omega/c}|C|^2=1. \tag{B3}$$

To evaluate the above sum we make the additional assumption that the lens collects $\mathbf{k}$ vectors propagating very close to the x-axis. In this *paraxial wave* limit, the sum can be converted to an integral as

$$\sum_{k=\omega/c}|C|^2=|C|^2\frac{L_yL_z}{(2\pi c)^2}\int d\theta\int d\phi\omega^2\sin\theta, \tag{B4}$$

where L_y and L_z are the length of the bounding box from the quantization of the free-space modes in the y and z directions, and angles θ and ϕ are defined in Fig. 2. From the above equation we attain

$$C = \frac{2\pi c}{\omega}\frac{1}{\sqrt{L_y L_z}}\frac{1}{\sqrt{A}}, \tag{B5}$$

where $A = 2\pi(\cos\Delta_i - \cos\Delta_o) \approx \pi(\Delta_o^2 - \Delta_i^2)$. Using this expression we then have

$$\beta(\omega) = \langle \mathbf{b}_\omega \rangle = \frac{2\pi c}{\omega}\frac{1}{\sqrt{L_y L_z}}\frac{1}{\sqrt{A}}\sum_{[\theta,\phi]\in[\Delta\phi,\Delta\theta]}\langle \hat{\mathbf{b}}_\mathbf{k}\rangle,$$

where $\hat{\mathbf{b}}_\mathbf{k}$ is given in Eq. (11). We again turn the sum into an integral and perform some algebraic manipulation to attain

$$\beta(\omega) = -\frac{d^2\omega^{3/2}\mathcal{L}(\delta_a,\gamma_a)\Omega(\omega)e^{-i\omega t}}{2c\gamma_a\sqrt{2\epsilon_0\hbar L_x A}}\int d\theta\int d\phi e^{i(\mathbf{k}_\omega-\mathbf{k})\cdot\mathbf{r}}, \tag{B6}$$

where angles θ and ϕ are illustrated in Fig. 2. We assume that the input pulse has a narrow bandwidth centered around ω_0 so that we may make the substitutions $\omega^{3/2} \approx \omega_0^{3/2}$ and $\exp(\mathbf{k}_\omega - \mathbf{k}) \approx \exp[k_0(\hat{\mathbf{x}} - \hat{\mathbf{k}})]$. We do not, however, make this approximation for $\mathcal{L}(\delta_a,\gamma_a)$ which is a rapidly varying function of ω near resonance. With these approximations we attain the result stated in Eqs. (16) and (17).

APPENDIX C: CALCULATION OF AVERAGE SCATTERING AMPLITUDE DUE TO ATOMIC RECOIL

We assume that the collection optics is frequency independent over the bandwidth of the collected signal. We assume quasimonochromatic input so that $\mathcal{L}(\delta_a,\gamma_a) = \gamma_a/[\gamma_a - i(\omega_a - \omega_0)]$. We can construct a fiber mode of the form

$$\hat{\mathbf{b}} = \sum_\omega \chi E^*(\omega)e^{i\omega t}\mathbf{b}_\omega, \tag{C1}$$

where χ is a normalization constant. This is the only mode that the collected field will couple to. To understand why, we first note that we can construct a complete basis using the above mode along with a set of other orthogonal modes that can be calculated using Schmidt decomposition. We can then calculate the field amplitude using

$$\langle\beta\rangle = \langle\hat{\mathbf{b}}\rangle = \sum_\omega \chi E^*(\omega)e^{i\omega t}\langle\beta(\omega)\rangle. \tag{C2}$$

Since $\beta(\omega)$ is proportional to the complex conjugate of the expansion coefficient $\chi E^*(\omega)e^{i\omega t}$, it will have a maximum overlap with the mode in Eq. (C1), and will be orthogonal to all other modes, ensuring the mode in Eq. (C1) is the only one that contains photons.

Unitarity determines the value of χ from

$$\sum_\omega |\chi|^2|E(\omega)|^2 = 1, \tag{C3}$$

which leads to

$$\chi = \frac{\pi c\sqrt{2\epsilon_0}}{\sqrt{L_x\hbar\omega_0}}\frac{1}{\sqrt{n}}. \tag{C4}$$

Plugging the above expression into Eq. (C2) and turning the sum into an integral we obtain

$$\langle\beta\rangle = B\int d\theta\int d\phi\langle e^{i(\mathbf{k}_{\omega_0}-\mathbf{k})\cdot\mathbf{r}}\rangle, \tag{C5}$$

where

$$B = \frac{-d^2\omega_0^2}{4\pi c^2\epsilon_0\hbar}\sqrt{\frac{n}{A}}\frac{\mathcal{L}(\delta_a,\gamma_a)}{\gamma_a} \tag{C6}$$

and, just as in Appendix B $A = 2\pi(\cos\Delta_i - \cos\Delta_o) \approx \pi(\Delta_o^2 - \Delta_i^2)$. We now use Eq. (33) to write

$$\langle\beta\rangle = B\int d\theta\int d\phi e^{-2\eta^2(1-\cos\hat{\theta}\cos\phi)(\bar{n}+1/2)}. \tag{C7}$$

Because we are working in the paraxial limit we can expand the exponent to second order in $\hat{\theta}$ and ϕ. Defining $\Delta = \sqrt{\hat{\theta}^2+\phi^2}$ we have

$$\int d\theta\int d\phi e^{-2\eta^2(1-\cos\hat{\theta}\cos\phi)(\bar{n}+1/2)} = 2\pi\int_{\Delta_i}^{\Delta_o} d\Delta\Delta e^{-\eta^2\Delta^2} = \frac{e^{-\eta^2\Delta_o^2} - e^{-\eta^2\Delta_i^2}}{\eta^2}. \tag{C8}$$

Taking the limit $\Delta_i \to 0$ and plugging into the above equation we attain the expression in Eq. (31).

Similarly, we can write

$$\langle|\beta|^2\rangle = |B|^2\int d\theta\int d\phi\int d\theta'\int d\phi'\langle e^{-(\mathbf{k}-\mathbf{k}')\cdot\mathbf{r}}\rangle. \tag{C9}$$

It is straightforward to show that the lowest-order contribution to the exponent is fourth order in θ, θ', ϕ, and ϕ'. Since we are only expanding to second order in these variables, we have

$$\langle|\beta|^2\rangle = |B|^2\int d\theta\int d\phi\int d\theta'\int d\phi' = |B|^2A^2, \tag{C10}$$

which leads directly to Eq. (31).

[1] A. Einstein, B. Podolsky, and N. Rosen, Phys. Rev. **47**, 777 (1935).

[2] E. Schrödinger, Proc. Cambridge Philos. Soc. **31**, 555 (1935).

[3] M. A. Nielsen and I. L. Chuang, *Quantum Computation and Quantum Information* (Cambridge University Press, Cambridge, UK, 2000).

[4] C. Monroe and M. Lukin, Phys. World **21**, 32 (2008).

[5] B. B. Blinov, D. L. Moehring, L.-M. Duan, and C. Monroe, Nature (London) **428**, 153 (2004).

[6] J. Sherson, B. Julsgaard, and E. S. Polzik, Adv. At., Mol., Opt.

Phys. **54**, 81 (2007).
[7] P. O. Schmidt, T. Rosenband, C. Langer, W. M. Itano, J. C. Bergquist, and D. J. Wineland, Science **309**, 749 (2005).
[8] L. M. Duan, M. D. Lukin, J. I. Cirac, and P. Zoller, Nature (London) **414**, 413 (2001).
[9] L. I. Childress, J. M. Taylor, A. Sorensen, and M. D. Lukin, Phys. Rev. Lett. **96**, 070504 (2006).
[10] E. Waks and J. Vuckovic, Phys. Rev. Lett. **96**, 153601 (2006).
[11] D. Sridharan and E. Waks, Phys. Rev. A **78**, 052321 (2008).
[12] D. L. Moehring, P. Maunz, S. Olmschenk, K. C. Younge, D. N. Matsukevich, L.-M. Duan, and C. Monroe, Nature (London) **449**, 68 (2007).
[13] C. W. Chou, H. de Riedmatten, D. Felinto, S. V. Polyakov, S. J. van Enk, and H. J. Kimble, Nature (London) **438**, 828 (2005).
[14] C.-W. Chou, J. Laurat, H. Deng, K. S. Choi, H. de Riedmatten, D. Felinto, and H. J. Kimble, Science **316**, 1316 (2007).
[15] K. S. Choi, H. Deng, J. Laurat, and H. J. Kimble, Nature (London) **452**, 67 (2008).
[16] X. Xu, B. Sun, P. R. Berman, D. G. Steel, A. S. Bracker, D. Gammon, and L. J. Sham, Nat. Phys. **4**, 692 (2008).
[17] D. Press, T. D. Ladd, B. Zhang, and Y. Yamamoto, Nature (London) **456**, 218 (2008).
[18] M. T. Rakher, N. G. Stoltz, L. A. Coldren, P. M. Petroff, and D. Bouwmeester, Phys. Rev. Lett. **102**, 097403 (2009).
[19] R. Blatt and D. Wineland, Nature (London) **453**, 1008 (2008).
[20] S. Olmschenk, K. C. Younge, D. L. Moehring, D. N. Matsukevich, P. Maunz, and C. Monroe, Phys. Rev. A **76**, 052314 (2007).
[21] K.-M. C. Fu, S. M. Clark, C. Santori, C. R. Stanley, M. C. Holland, and Y. Yamamoto, Nat. Phys. **4**, 780 (2008).
[22] U. Eichmann, J. C. Bergquist, J. J. Bollinger, J. M. Gilligan, W. M. Itano, D. J. Wineland, and M. G. Raizen, Phys. Rev. Lett. **70**, 2359 (1993).
[23] W. M. Itano, J. C. Bergquist, J. J. Bollinger, D. J. Wineland, U. Eichmann, and M. G. Raizen, Phys. Rev. A **57**, 4176 (1998).
[24] X.-F. Zhou, Y.-S. Zhang, and G.-C. Guo, Phys. Rev. A **71**, 064302 (2005).
[25] S. Hughes and H. Kamada, Phys. Rev. B **70**, 195313 (2004).
[26] D. Englund, A. Faraon, I. Fushman, N. Stoltz, P. Petroff, and J. Vuckovic, Nature (London) **450**, 857 (2007).
[27] K. Srinivasan and O. Painter, Nature (London) **450**, 862 (2007).
[28] M. V. G. Dutt *et al.*, Phys. Rev. Lett. **94**, 227403 (2005).
[29] X. Xu, W. Yao, B. Sun, D. G. Steel, A. S. Bracker, D. Gammon, and L. J. Sham, Nature (London) **459**, 1105 (2009).
[30] C. Latta *et al.*, Nat. Phys. **5**, 758 (2009).
[31] I. T. Vink, K. C. Nowack, F. H. L. Koppens, J. Danon, Y. V. Nazarov, and L. M. K. Vandersypen, Nat. Phys. **5**, 764 (2009).
[32] W. K. Wootters, Phys. Rev. Lett. **80**, 2245 (1998).
[33] M. B. Plenio and S. Virmani, Quantum Inf. Comput. **7**, 1 (2007).
[34] A. S. Bracker *et al.*, Phys. Rev. Lett. **94**, 047402 (2005).
[35] N. D. Mermin, J. Math. Phys. **7**, 1038 (1966).
[36] D. S. Bateman, S. K. Bose, B. Dutta-Roy, and M. Bhattacharyya, Am. J. Phys. **60**, 829 (1992).